Desert pavements stabilise arid vegetation patterns

Ida Gaulke[1], Alisha Matheson[1], Leloba Jefferis[1], Dominik Nommensen[1], Josh Evans[1], Victoria M. Fernandes[1], David Dunkerley[1], Patrick Taggart[2], Andrew Gunn[1,*]

[1]School of Earth, Atmosphere and Environment, Monash University, Clayton, Victoria 3800, Australia

[2]Bush Heritage Australia, Docklands, Victoria 3008, Australia

[*]a.gunn@monash.edu

Abstract

Some vegetation patterns have aridity-dependent morphology[1]. On low-angle arid hillslopes, vegetation organises into bands which follow topographic contours[2]. Terraces emerge with these bands due to vegetation's drag on sediment-laden runoff[3], creating a topographic signature of life[4] diagnostic of precipitation rate[5]. Another widespread feature of arid environments is desert pavement, surficial pebbles that armour finer-grained sediments, which is considered a hallmark of landscape stability[6]. Banding and pavement often co-occur[7,8], however their interaction has not been studied. Here we show that vegetation-induced topographic terracing is stabilised by pavement development. In proximal field sites with varying pavement coverage, we illustrate that pavements suppress seed germination and reduce sediment erosion between vegetation bands, stabilising terrace morphology. Despite sites experiencing consistent contemporary precipitation, they exhibit relationships between terrace morphology, topographic slope, and band spacing consistent with patterns formed under wetter conditions at sites with greater pavement coverage, implying aridity has increased as pavements emerged. This suggests that pavements preserve terracing and spacing diagnostic of paleoprecipitation. Because pavement age[6], band spacing[9], and topographic slopes are readily observable, we believe our study identifies a new widespread paleo-precipitation proxy in arid environments where conventional alternatives are often unattainable[10].

Main text

Periodic vegetation patterns are highly sensitive to climatic shifts[2,11]. Banded vegetation appears as laterally continuous vegetated bands (or 'groves') separated by bare interbands (or 'intergroves') that extend along topographic contours on shallow hillslopes[12] (Fig. 1, Extended Data Fig. 1). Runoff-runon processes drive the persistence of these bands in which overland water flow runs off from highly impermeable interbands and infiltrates into permeable, vegetated bands[13]. Observed upslope germination and downslope senescence (plant decay) are thought to be a spatial depiction of the temporal upslope migration of bands[14], and evidence of this phenomenon is mostly restricted to models[15–17]. Gradients in downslope sediment transport, produced by the overland flow that maintains the pattern, can generate a stepped terrace microtopography[18] with flatter, eroding interbands and steeper, depositional bands (Fig. 1g).

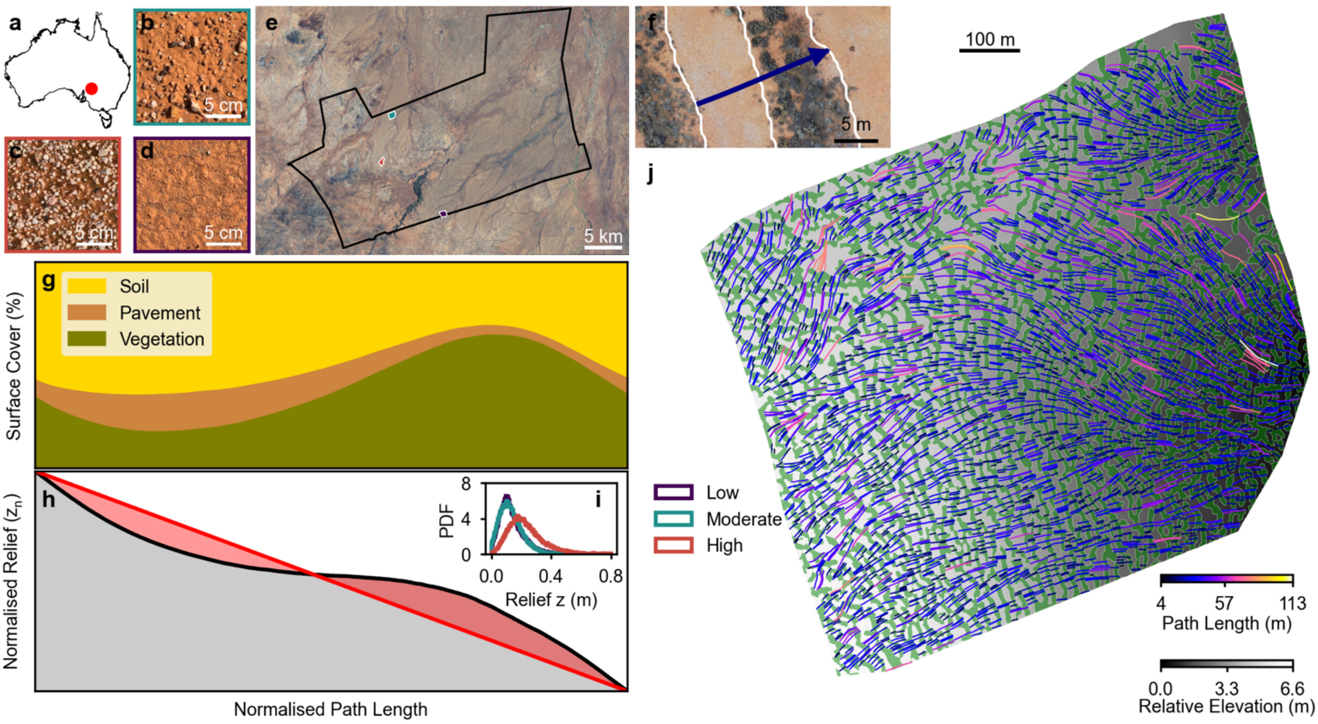

Fig. 1: Study site and methodology. a, Location of Boolcoomatta Reserve within Australia (red dot). Representative interband surface images of sites showing **b,** Moderate, **c,** High, and **d,** Low site desert pavement fractions. **e,** Satellite image of Boolcoomatta Reserve (black outline) with the three study sites marked (colours as **b-d**). **f,** An example downslope path (blue, 16.2 m) from **j** on orthomosaic, defined from the top of an interband (left) and finishing at the bottom of a band (right), and automatically defined band edges (white). **g,** Stacked median surface cover fraction across normalised path length for all paths in the Moderate site. **h,** Normalised median downslope profile (black), for all paths in the Moderate site, with red shaded area indicating the terracing metric. **i,** Probability density function (PDF) histogram of relief for paths in each site, with sites coloured as in **e**. **j,** Example map of the Moderate site showing relative elevation (grey shading) and vegetation bands (translucent green). Automatically defined downslope paths (only 1/20th shown for clarity) coloured by path length. For **a**, **e**, **f**, and **j**, north is orientated upward. Scale bars provided for **b-e, i** and **j**.

Previous research has not considered the influence of desert pavement (or 'gibber'; Fig. 1b-d)—widespread in arid regions[8] and thought to be a hallmark of surface stability[19–21]—on band migration or terrace development in these systems. The production and distribution of these pebble-sized clasts that mantle some interbands in a monolayer[22] is poorly understood. Desert pavement is known to significantly alter soil surface conditions in non-banded environments[23–26], and while this is likely also true for pavement in banded vegetation, no study has yet addressed these implications with regard to the temporal development of these systems. Here, we present evidence demonstrating the influence of desert pavements on banded vegetation development from three sites across Boolcoomatta Reserve with equivalent precipitation (Fig. 1a,e,j; Extended Data Fig. 2-3; Methods M1). The reserve is located on Australia's arid fringe, a region that has been subject to substantial climatic shifts during glacial-interglacial cycles[19,27,28].

Banded vegetation morphology

Using UAV LiDAR (Methods M2), we observe terracing associated with vegetation banding (Fig. 1g), and desert pavement forming in the interbands of these systems (Fig. 1f; Extended Data Fig. 4; Methods M3). Desert pavement is most prevalent at the High site, moderately abundant at the Moderate site, and largely absent at the Low site (Fig. 1b-d). The median relief of one wavelength of the pattern is 0.15 m, with the High site exhibiting both the greatest variation and the largest values of path relief (Fig. 1h).

For constant slope, band spacing (Fig. 2a-c, Methods M4-5) and terracing (Fig. 2d-f, Methods M6) increase with interband desert pavement, although the magnitude of this relationship differs between sites. The results also reveal substantial inter-site differences in band spacing and terracing (Fig. 2g), where the High site supports banded vegetation with a narrower, flatter morphology compared to the Low and Moderate sites which have wider bands with a more pronounced stepped topography. The Moderate site exhibits both the largest band spacing and terracing.

It is well understood that slope has an inverse relationship with band spacing[2,29,30] as overland flow becomes less efficient on lower slopes, delivering less water to vegetated bands, a finding reflected in our results for constant interband pavement fraction. The presence of a desert pavement mantle may produce a similar effect by increasing drag on overland flow[31], thereby reducing the water reaching vegetated bands. This would increase water residence time, and therefore infiltration in the interbands, forcing band spacing to widen to maintain vegetation.

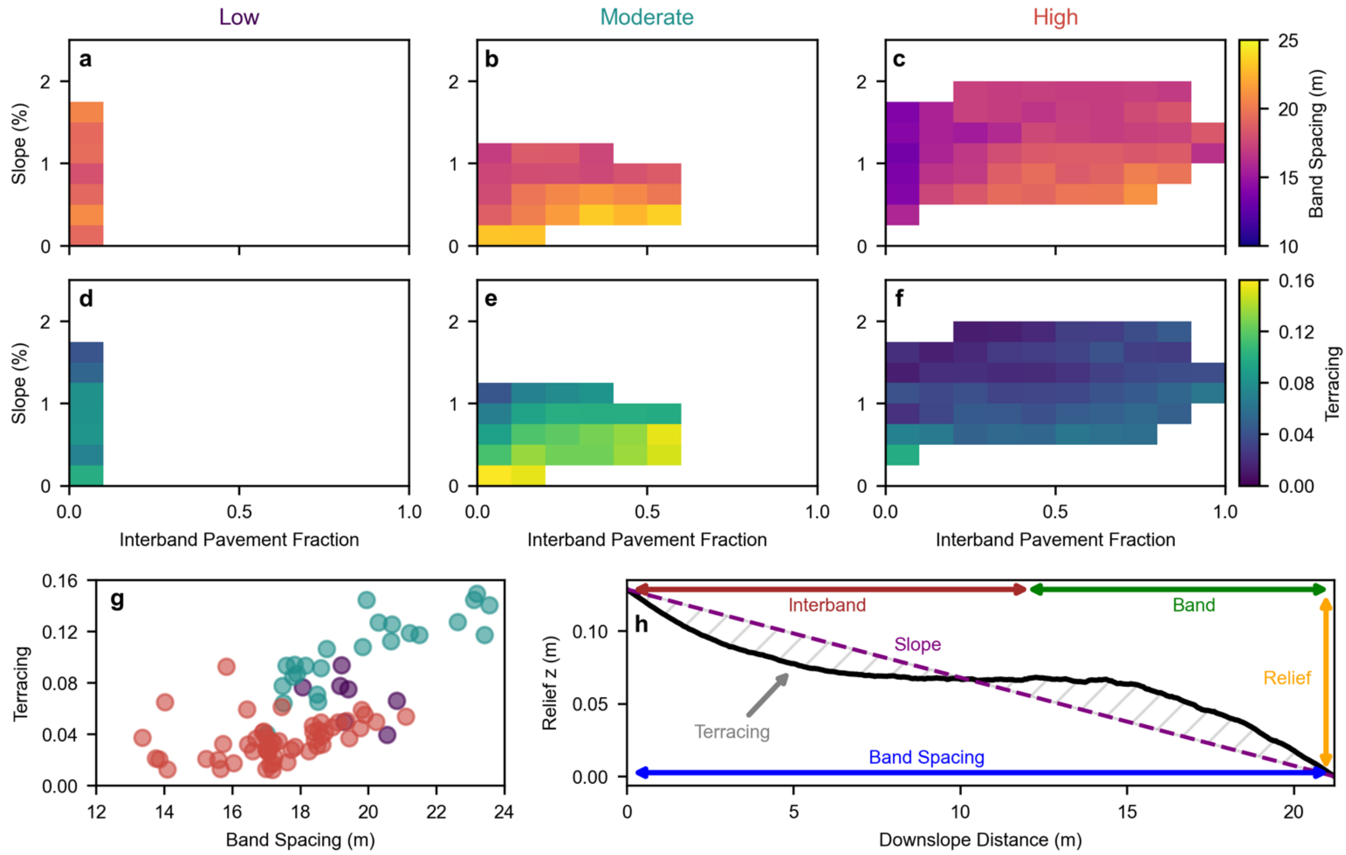

Fig. 2: Banded vegetation morphology as a function of slope and interband desert pavement fraction. Median **a-c**, band spacing and **d-f**, terracing across slope and interband pavement fraction bins, for the three sites (columns; labelled above, with titles coloured as in Fig. 1). **g,** Scatterplot of band spacing and terracing, showing the median value for paths within each pavement fraction and slope bin in **a-f**. Points are coloured by site as above. **h,** Annotated median profile (black line) of the Moderate site for 35% ± 5% interband desert pavement fraction and 0.625% ± 0.125% slope (2,371 paths). Median interband (brown) and band (green) width, band spacing (blue), relief (yellow), terracing (grey hatching), and slope (purple dashed line) variables are indicated. For **a-g**, only bins containing more than 0.5% of all paths within that site are shown (Low: 67,065 paths; Moderate: 79,740 paths; High: 57,034 paths).

The effect of pavement on terracing is more complex. The positive relationship between terracing and pavement fraction may imply that terrace formation accelerates pavement development, potentially via argillipedoturbation (or 'shrink-swell') processes[32,33] that lever clasts upward during cyclic soil expansion and contraction (Extended Data Fig. 5). By reducing interband slopes and increasing water retention[30], terraces likely intensify the wetting-drying cycles that drive this vertical particle transport. However, the absence of deep cracking[34,35] in interbands, observed within vegetated bands (Extended Data Fig. 6), challenges this mechanism. Alternatively, erosion associated with terrace formation may lower interband surfaces to reveal subsurface pebbles, exhuming the pavement rather than uplifting it[33].

Terracing in banded vegetation is a measure of band persistence and stability[36] generated by gradients in sediment flux[37,38]. Analogous to a Froude number transition, terrace morphology reflects the competition between the upslope 'wave' of vegetation band migration and the downslope 'flow' of sediment. When these rates are near-equal, terraces remain small because vegetation cannot stabilise the sediment flux long enough to build significant relief[39]. Because we find that terrace relief increases with pavement cover (Fig. 2d-f), we infer that desert pavement has a stabilising effect on banded vegetation systems, immobilising bands and allowing the accumulation of sediment in terraces[30]. However, we still see differences between sites for constant pavement and slope.

Surface sediment characteristics

To explain these inter-site differences, we analysed surface sediment characteristics (Extended Data Fig. 3a-c, Methods M7), finding that non-pavement near-surface sediment in the Moderate site interbands is coarser than that of the Low site (Fig. 3a). Unlike finer-grained sediment that coheres to form hard surface crusts, this coarser sediment remains readily transportable by overland flow[40], thereby accelerating terrace development. The coarser substrate also increases soil permeability, enhancing infiltration across the interband. This supports the wider band spacing that we see in the Moderate site, exacerbated by the presence of the terraces themselves, which reduce both the interband slope and overland flow capacity.

In contrast, because only a small fraction of the High site dataset falls within the lowest interband pavement fraction bin (Extended Data Fig. 7, Extended Data Table 1), a direct comparison with the Low site is unfeasible. The High site overlaps more significantly with the Moderate site, where sediment is marginally finer and less sorted (Fig. 3a). While these more permeable sediments should generate wider band spacing and larger terraces in the Moderate site, we observe the opposite trend (Fig. 2g). We therefore suggest that the emergence of the pavement (Fig. 3b) is the catalyst for this morphological disparity.

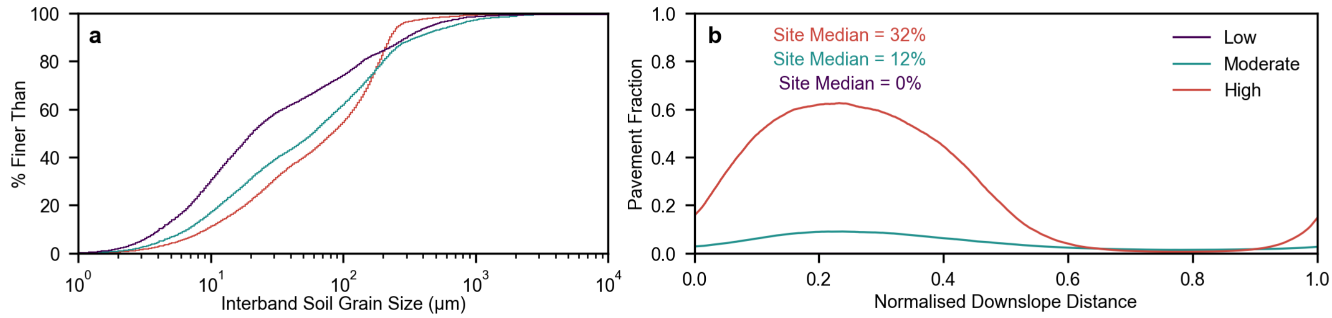

Fig. 3: Surface sediment characteristics. a, Cumulative grain size distribution of interband surface sediment samples. Lines are coloured as in **b**: Low (purple), Moderate (cyan), High (brown). **b,** Median desert pavement fraction across a normalised downslope profile where 0 is the upslope margin of an interband and 1 is the downslope margin of a band. Annotations indicate the fraction of total valid site area (Extended Data Fig 3) covered by desert pavement.

System stabilisation

Because terrace relief scales with desert pavement fraction, we surmise that the presence of pavement has a stabilising effect on the migration of banded systems. Our results indicate that the fraction of vegetation growing within interbands is inversely related to the amount of interband desert pavement (Fig. 4a; Extended Data Fig. 8). Several studies have shown that desert pavement armours the surface, creating xeric, inhospitable environments for plant germination[1,41–43]. These surfaces have high bulk densities[30,44], reducing the rate and depth of infiltration[26,41], and creating a physical restriction to root penetration[30]. Additionally, these pavemented surfaces have low unsaturated hydraulic conductivity[35], restricting the amount of water that can reach the surface by capillary rise. We therefore interpret that the inability of plants to germinate in pavemented interbands stabilises these paved systems by halting upslope migration of bands, as pioneer species are no longer able to colonise the lower interband[9].

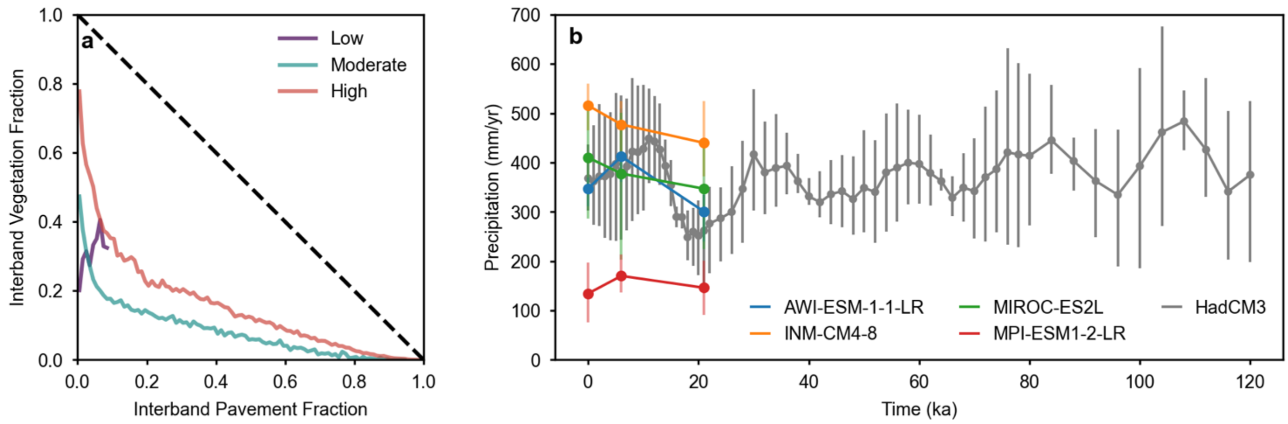

Fig. 4: Interband surface cover relationships and modelled palaeoprecipitation. **a,** Median interband vegetation fraction as a function of interband desert pavement fraction, calculated within pavement-fraction bins for each site (Low, Moderate, High). The dashed line demonstrates the complementary cover relationship (vegetation fraction = 1 - pavement fraction). **b,** Modelled mean annual regional precipitation from five climate models[45–48] spanning the last Pleistocene to the present (Methods M8). Points show model means for each time slice, vertical bars indicate the interquartile range across monthly values.

As band spacing depends on precipitation—a drier environment forces the spacing to increase as a longer fetch is required to sustain the vegetation in the bands[12,49]—this armouring effect may also prevent band spacing from adjusting to subsequent changes in precipitation. This may explain why the band spacing in the High site is narrower than that of the Moderate site (Fig. 2g), despite the understanding that a higher desert pavement fraction should result in a wider spacing. Instead, once the pavement reaches a critical fraction, the extensive surface cover impedes the ability of the vegetation bands to adjust to subsequent changes in regional precipitation, preserving a legacy configuration.

Terrace relief reflects the balance between band migration and downslope sediment transport, thus providing a proxy for pattern mobility. Applying this framework to our results, we would expect to see large terraces in the High site where the sediment is most transportable (Fig. 3a), and the pavement fraction is greatest (Fig. 3b), thus the pattern is the most stable. However, we find the opposite, suggesting instead that a sufficiently high pavement mantle also influences sediment transport (Extended Data Fig. 9). This idea is supported by several studies determining that pavement mantles reduce sediment transport through both a supply limitation[50,51], by covering erodible grains, and a transport limitation[52], as pebbles increase resistance to overland flow. Indeed, the presence of large terraces in the Moderate site (Fig. 2e), where there is less desert pavement cover, may result from a combination of sediment transportability and desert pavement surface armouring. The lower pavement cover fraction may reduce downslope sediment transport without fully inhibiting it. This partial stabilisation of band positions relative to sediment transport could allow terraces to continue building over time, although the relative importance of these mechanisms remains unclear.

Evidence of aridification?

Given these findings, we propose that these systems may illustrate evidence of aridification. The narrower band spacing in the High site (Fig. 2) suggests that the desert pavement mantle may have reached a stabilising cover fraction during a wetter climatic period, as more rainfall would have been necessary to generate the observed band spacing[12]. The Moderate site, partially stabilised by an intermediate cover of desert pavement, likely reflects drier interim conditions, evidenced by the wider band spacing. However, it may retain some capacity to adapt to changes in precipitation. The Low site by contrast, with minimal desert pavement, is theorised to be in equilibrium with the current regional precipitation conditions, modulated by its finer sediment composition.

Testing this hypothesis remains challenging due to the lack of age constrains on when desert pavement reached a cover threshold sufficient to stabilise the vegetation pattern, compounded by disagreements among selected coupled paleoclimate models (Fig. 4b). Obtaining absolute ages for pavement emplacement in the landscape would assist in constraining which models accurately reflect the trend in precipitation. For example, HadCM3 could be consistent if pavement development occurred in the High and Moderate sites sometime since ~15 ka, prior to the modelled decline in precipitation.

In addition, a quantitative relationship between precipitation and band spacing is yet to be established[53]. If such a relationship can be established, alongside an evolutionary model for desert pavement cover, pavemented banded vegetation patterns may serve as a novel geomorphic archive of paleoclimate in arid regions where conventional proxies are often absent. Furthermore, the presence of desert pavement preserves the magnitude of terracing in the system, providing a signature of band migration prior to the pavement maturation. If dated, terraces may provide insight into the duration of band stability and the rate of desert pavement development.

The findings help us understand the broader implications for how these arid landscapes evolve over time by providing clues about the environmental factors that influence the pattern expression. This is essential for understanding climate dynamics and the history of human occupation across Australia, as well as for conservation efforts aimed at preserving these striking ecosystems.

Methods

M1. Study area

Boolcoomatta Reserve is a 63,000-hectare conservation property in central-eastern South Australia (Fig. 1a), located on the traditional lands of the Adnyamathanha & Wilyakali people, actively managed by Bush Heritage Australia. The reserve has an arid climate and receives an average of 190 mm of annual precipitation, with substantial interannual variability[54]. The geology is comprised of Precambrian igneous and metamorphic bedrock, with eroding outcrops visible in places, overlain by sedimentary rocks from the Mesozoic and Tertiary periods[55]. At the surface, sub-sand-sized sediments are interspersed with weathering-resistant quartz and iron oxide concretion pebbles which form the desert pavement[56].

The landscape is dominated by extensive chenopod shrublands on low-angle slopes, associated with gilgai soils dissected by ephemeral drainage channels[55]. These shrublands support the banded vegetation on the reserve. Three banded vegetation sites, Low, Moderate, and High, referring to their bulk pavement fraction, were selected across the property to capture the variability in vegetation banding and desert pavement cover (Fig. 1b-e). The Low site has a consistent, shallow slope with wide band spacing, and a minimal pavement surface fraction. The Moderate site has variable slope around dissecting ephemeral drainage channels, wide band spacing, and a moderate pavement surface fraction. The High site has a consistent, steeper slope with narrow band spacing, and a high pavement surface fraction. Differences in the long-term rainfall between sites are assumed negligible due to their proximity (Fig. 1e). The site boundaries were defined either by the extent of continuous vegetation bands or by a maximum site size of 710,000 m^2, constrained by drone flight time restrictions.

M2. Data collection

A DJI M350 drone flown over each study area at 8 m/s and 100 m altitude captured LiDAR and imagery data using a nadir-pointing Zenmuse L1 sensor in parallel paths. A digital terrain model (DTM) was produced using minimum-elevation LiDAR points with less than 10° azimuth at 0.5-m resolution, and an RGB orthomosaic was produced at 2.5-cm resolution. All data was projected in EPSG 32754.

M3. Surface type classification

Typical RGB values for soil (open and bioturbated), vegetation (shrubs and herbs), gibber, and shadow were manually identified for each study area orthomosaic. Each 2.5-cm wide pixel was then type-classified using minimum distance in RGB-space, then this raster was coarsened at 0.5-m resolution to fractional-type, excluding shadows, aligned with the DTM (Extended Data Fig. 3).

M4. Band identification

Bands were identified by first computing pixels where the vegetation fraction smoothed (using FFT convolution with a circular kernel) at 5-m radius exceeded that smoothed at 10-m radius. Connected regions smaller than $5^2\pi$ m^2 were removed, and only those where the 75th percentile vegetation fraction exceeded 0.5 were retained as bands. Band boundaries were sampled at 0.5-m intervals, and boundary segments were classified as upslope or downslope edges based on whether the inward-pointing edge normal was within 90° of the local topographic dip direction (20-m radius smoothed).

M5. Path identification

Paths were defined downslope along local 20-m radius smoothed dip between pairs of downslope band edges, where along-path length of band and interband each exceed 2 m. Per band, paths were calculated every 0.5-m along downslope band edges. Properties such as surface cover and elevation were then interpolated from rasters onto 400 equidistant steps along paths which cover one pattern wavelength (Fig. 1i).

M6. Terracing degree

The degree of terracing was defined as the integral of the absolute residual between the normalised topography profile and $z/\eta=-x/L$, where η is the terrace relief over its wavelength L (Fig. 1g). This number therefore varies strictly between 0 and 1 but with a realistic maximum of 0.5.

M7. Sediment sampling

Sediment samples from <5-cm depth were collected from the midpoint of 3 interbands along a transect in each site (Extended Data Fig. 3a-c). Samples were prepared using a sieve stack to remove organic matter, then soaked in a 3% sodium hexametaphosphate solution to deflocculate grains. Samples were then stirred and passed through a 250-micron sieve to separate the fine and coarse fraction. The fine fraction was analysed using a Camsizer X2 X-Flow module, while the coarse fraction was dried and analysed using a Camsizer X2 X-Fall module. All reasonable care was taken to reduce the unintentional loss of dust as sediment was moved. The two grain size distributions were merged based on the initial mass fraction of the fine and coarse subsamples.

M8. Climate model precipitation

Monthly precipitation predictions from the 4 CMIP6/PMIP4 Earth System Models (ESM) with data available across all 3 of the 'historical'[45] (0 ka), 'midHolocene'[46] (6 ka), and 'lgm'[47] (21 ka) scenarios (AWI-ESM-1-1-LR, MIROC-ES2L, INM-CM4-8, and MPI-ESM1-2-LR), and the HadCM3 ESM for intervals over the last 120 ka[48], were averaged over a spatial region of 34°S-28°S and 136°E-144°E around the study area (larger due to model resolution).

Data availability

Data during the review process is available here and will be provided with a DOI on acceptance.

Code availability

Code during the review process is available here and will be provided with a DOI on acceptance.

References

1. Kéfi, S. *et al.* Spatial vegetation patterns and imminent desertification in Mediterranean arid ecosystems. *Nature* 449, 213–217 (2007).
2. Valentin, C., d'Herbès, J. M. & Poesen, J. Soil and water components of banded vegetation patterns. *Catena (Amst).* 37, 1–24 (1999).
3. Van Dijk, P. M., Kwaad, F. J. P. M. & Klapwijk, M. Retention of water and sediment by grass strips. *Hydrol. Process.* 10, 1069–1080 (1996).
4. Dietrich, W. E. & Perron, J. T. The search for a topographic signature of life. *Nature* 439, 411–418 (2006).
5. Klausmeier, C. A. Regular and Irregular Patterns in Semiarid Vegetation. *Science (1979).* 284, 1826–1828 (1999).
6. Matmon, A. *et al.* Desert pavement-coated surfaces in extreme deserts present the longest-lived landforms on Earth. *Bulletin of the Geological Society of America* 121, 688–697 (2009).
7. Deblauwe, V., Barbier, N., Couteron, P., Lejeune, O. & Bogaert, J. The global biogeography of semi-arid periodic vegetation patterns. *Global Ecology and Biogeography* 17, 715–723 (2008).
8. Brenning, A., Güldner, L., Schepanski, K., Dietze, M. & Fuchs, M. Geomorphic Distribution Modeling of Desert Pavements: Towards a Global Assessment. in *Geomorphometry* 1–4 (Zenodo, Perugia, Italy, 2025).
9. Deblauwe, V., Couteron, P., Bogaert, J. & Barbier, N. Determinants and dynamics of banded vegetation pattern migration in arid climates. *Ecol. Monogr.* 82, 3–21 (2012).
10. Weij, R. *et al.* Elevated Southern Hemisphere moisture availability during glacial periods. *Nature* 626, 319–326 (2024).
11. Tongway, D. & Ludwig, J. Theories on the Origins, Maintenance, Dynamics, and Functioning of Banded Landscapes. in *Banded Vegetation Patterning in Arid and Semiarid Environments: Ecological Processes and Consequences for Management* (eds. Tongway, D., Valentin, C. & Seghieri, J.) vol. 149 36 (Springer-Verlag, New York, 2001).
12. Valentin, C. & d'Herbes, J. M. Niger tiger bush as a natural water harvesting system. *Catena (Amst).* 37, 231–256 (1999).
13. Macfadyen, W. A. Soil and Vegetation in British Somaliland. *Nature* 165, 121–121 (1950).
14. Delcourt, P. A. & Delcourt, H. R. Ecotone Dynamics in Space and Time. in *Landscape Boundaries* (eds. Hansen, A. & di Castri, F.) vol. 92 19–54 (Springer International Publishing, New York, 1992).
15. Esteban, J. & Fairén, V. Self-organized formation of banded vegetation patterns in semi-arid regions: A model. *Ecological Complexity* 3, 109–118 (2006).
16. Pinto-Ramos, D., Clerc, M. G. & Tlidi, M. Topological defects law for migrating banded vegetation patterns in arid climates. *Sci. Adv.* 9, 1–11 (2023).
17. Dunkerley, D. Banded vegetation in some Australian semi-arid landscapes: 20 years of field observations to support the development and evaluation of numerical models of vegetation pattern evolution. *Desert* 23, 165–187 (2018).
18. Mabbutt, J. A. & Fanning, P. E. Vegetation banding in arid Western Australia. *J. Arid Environ.* 12, 41–59 (1987).
19. Fujioka, T. *et al.* Global cooling initiated stony deserts in central Australia 2-4 Ma, dated by cosmogenic 21Ne-10Be. *Geology* 33, 993–996 (2005).
20. Fisher, A., Fink, D., Chappell, J. & Melville, M. 26Al/10Be dating of an aeolian dust mantle soil in western New South Wales, Australia. *Geomorphology* 219, 201–212 (2014).
21. Seong, Y. B., Dorn, R. I. & Yu, B. Y. Evaluating the life expectancy of a desert pavement. *Earth. Sci. Rev.* 162, 129–154 (2016).
22. Bromley, J., Brouwer, J., Barker, A. P., Gaze, S. R. & Valentin, C. The role of surface water redistribution in an area of patterned vegetation in a semi-arid environment, south-west Niger. *J. Hydrol. (Amst).* 198, 1–29 (1997).
23. Poesen, J. W., Torri, D. & Bunte, K. Effects of rock fragments on soil erosion by water at different spatial scales: a review. *Catena (Amst).* 23, 141–166 (1994).
24. Katra, I., Lavee, H. & Sarah, P. The effect of rock fragment size and position on topsoil moisture on arid and semi-arid hillslopes. *Catena (Amst).* 72, 49–55 (2008).
25. Ma, D. & Shao, M. Simulating infiltration into stony soils with a dual-porosity model. *Eur. J. Soil Sci.* 59, 950–959 (2008).
26. Assouline, S., Kamai, T., Svoray, T. & Narkis, K. Understanding the dynamics of evaporation from stony soils via laboratory experiments and numerical modeling. *J. Hydrol. (Amst).* 622, 129708 (2023).
27. Byrne, M. *et al.* Birth of a biome: Insights into the assembly and maintenance of the Australian arid zone biota. *Mol. Ecol.* 17, 4398–4417 (2008).
28. Hesse, P. P., Magee, J. W. & van der Kaars, S. Late Quaternary climates of the Australian arid zone: A review. *Quaternary International* 118–119, 87–102 (2004).
29. Eddy, J., Humphreys, G. S., Hart, D. M., Mitchell, P. B. & Fanning, P. C. Vegetation arcs and litter dams: similarities and differences. *Catena (Amst).* 37, 57–73 (1999).
30. Pelletier, J. D. *et al.* How do vegetation bands form in dry lands? Insights from numerical modeling and field studies in southern Nevada, USA. *J. Geophys. Res. Earth Surf.* 117, F04026 (2012).
31. Abrahams, A. D. & Parsons, A. J. Hydraulics of interrill overland flow on stone-covered desert surfaces. *Catena (Amst).* 23, 111–140 (1994).
32. Mabbutt, J. Stone distribution in a stony tableland soil. *Soil Research* 3, 131 (1965).

33. Dan, J., Yaalon, D. H., Moshe, R. & Nissim, S. Evolution of Reg soils in southern Israel and Sinai. *Geogerma* 28, 173–202 (1982).
34. Moeyersons, J., Nyssen, J., Poesen, J., Deckers, J. & Mitiku Haile. On the origin of rock fragment mulches on Vertisols: A case study from the Ethiopian highlands. *Geomorphology* 76, 411–429 (2006).
35. Poesen, J. & Lavee, H. Rock fragments in top soils: significance and processes. *Catena (Amst).* 23, 1–28 (1994).
36. Boaler, S. B. & Hodge, C. A. H. Observations on Vegetation Arcs in the Northern Region, Somali Republic. *J. Ecol.* 52, 511–544 (1964).
37. Exner, F. M. Zur physik der dünen. *Abhandlungen der Akadamie der Wissenschaften, Wien* 129(2a), 929–952 (1920).
38. Exner, F. M. Uber die wechselwirkung zwischen wasser und geschiebe in flussen. *Abhandlungen der Akadamie der Wissenschaften, Wien* 134(2a), 165–203 (1925).
39. Baartman, J. E. M., Temme, A. J. A. M. & Saco, P. M. The effect of landform variation on vegetation patterning and related sediment dynamics. *Earth Surf. Process. Landf.* 43, 2121–2135 (2018).
40. Hjulström, F. Studies of the morphological activity of rivers as illustrated by the River Fyris. *Bulletin of the Geological Institution of the University of Upsala* 25, 221–527 (1935).
41. Valentin, C. Surface sealing as affected by various rock fragment covers in West Africa. *Catena (Amst).* 23, 87–97 (1994).
42. Chappell, A. *et al.* Testing the validity of upslope migration in banded vegetation from south-west Niger. *Catena (Amst).* 37, 217–229 (1999).
43. Elvidge, C. D. & Iverson, R. M. Regeneration of Desert Pavement and Varnish. in *Environmental Effects of Off-Road Vehicles* (eds. Webb, R. H. & Wilshire, H. G.) 225–243 (Springer, New York, 1983). doi:10.1007/978-1-4612-5454-6_11.
44. Dunkerley, D. L. & Brown, K. J. Banded vegetation near Broken Hill, Australia: significance of surface roughness and soil physical properties. *Catena (Amst).* 37, 75–88 (1999).
45. Otto-Bliesner, B. L. *et al.* The PMIP4 contribution to CMIP6 - Part 2: Two interglacials, scientific objective and experimental design for Holocene and Last Interglacial simulations. *Geosci. Model Dev.* 10, 3979–4003 (2017).
46. Kageyama, M. *et al.* The PMIP4 contribution to CMIP6 - Part 4: Scientific objectives and experimental design of the PMIP4-CMIP6 Last Glacial Maximum experiments and PMIP4 sensitivity experiments. *Geosci. Model Dev.* 10, 4035–4055 (2017).
47. Eyring, V. *et al.* Overview of the Coupled Model Intercomparison Project Phase 6 (CMIP6) experimental design and organization. *Geosci. Model Dev.* 9, 1937–1958 (2016).
48. Davies-Barnard, T., Ridgwell, A., Singarayer, J. & Valdes, P. Quantifying the influence of the terrestrial biosphere on glacial-interglacial climate dynamics. *Climate of the Past* 13, 1381–1401 (2017).
49. Chen, Z., Wu, Y.-P., Feng, G.-L., Qian, Z.-H. & Sun, G.-Q. Effects of global warming on pattern dynamics of vegetation: Wuwei in China as a case. *Appl. Math. Comput.* 390, 125666 (2021).
50. Li, L. *et al.* Evolution of rock cover, surface roughness, and its effect on soil erosion under simulated rainfall. *Geoderma* 379, 114622 (2020).
51. Xia, L. *et al.* Effects of rock fragment cover on hydrological processes under rainfall simulation in a semi-arid region of China. *Hydrol. Process.* 32, 792–804 (2018).
52. Abrahams, A. D. & Parsons, A. J. Resistance to Overland Flow on Desert Pavement and Its Implications for Sediment Transport Modeling. *Water Resour. Res.* 27, 1827–1836 (1991).
53. Deblauwe, V., Couteron, P., Lejeune, O., Bogaert, J. & Barbier, N. Environmental modulation of self-organized periodic vegetation patterns in Sudan. *Ecography* 34, 990–1001 (2011).
54. Bureau of Meteorology (BoM). Climate Data Online. *Australian Government* http://www.bom.gov.au/climate/data/ (2023).
55. Wakelin-King, G. *Boolcoomatta Station Landscape Analysis & Rehabilitation of Surface Waters: A Report from Wakelin Associates to Bush Heritage Australia*. (2009).
56. Cowley, W. M. Geological Map South Australia. (Department for Energy and Mining, 2020).
57. Beck, H. E. *et al.* High-resolution (1 km) Köppen-Geiger maps for 1901–2099 based on constrained CMIP6 projections. *Sci. Data* 10, 724 (2023).

Acknowledgements

We acknowledge the Adnyamathanha, Wilyakali, and Bunurong Peoples as the Traditional Owners of the lands on which this research was conducted. We thank Bush Heritage Australia for in-kind support and facilitating field research, especially Tim Zwiersen, Donna Gaskin, and Graeme Finlayson. I.G. acknowledges the Linnean Society of New South Wales for the Betty Mayne Scientific Research Fund for Earth Sciences Grant. This research was undertaken with the assistance of resources from the National Computational Infrastructure (NCI Australia), an NCRIS enabled capability supported by the Australian Government (#NCMAS-2025-120).

Ethics declaration

The authors declare no competing interests.

Author contributions

Conceptualization, Data curation, Funding acquisition, Methodology, Project administration, I.G & A.G.; Formal analysis, Software, Validation, Writing – original draft, I.G.; Visualization, I.G. & D.N.; Investigation, Resources, Writing – review & editing, all authors; Supervision, A.G.

Extended Data

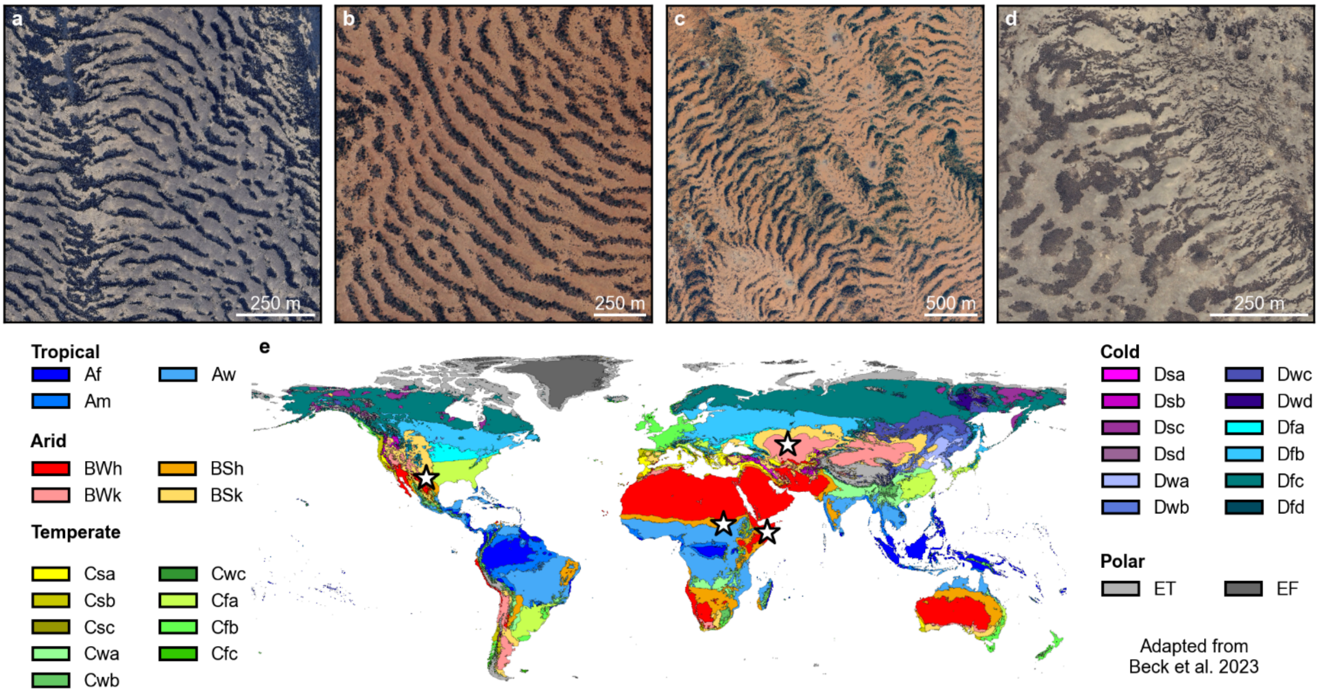

Extended Data Fig. 1: Banded vegetation examples. Banded vegetation systems in **a,** the United States of America, **b,** Sudan, **c,** Ethiopia, and **d,** Kazakhstan. Their locations are shown on a **e,** Köppen-Geiger climate map[57]. Satellite images are from Google Earth Pro. North is orientated upwards, scale bars are provided.

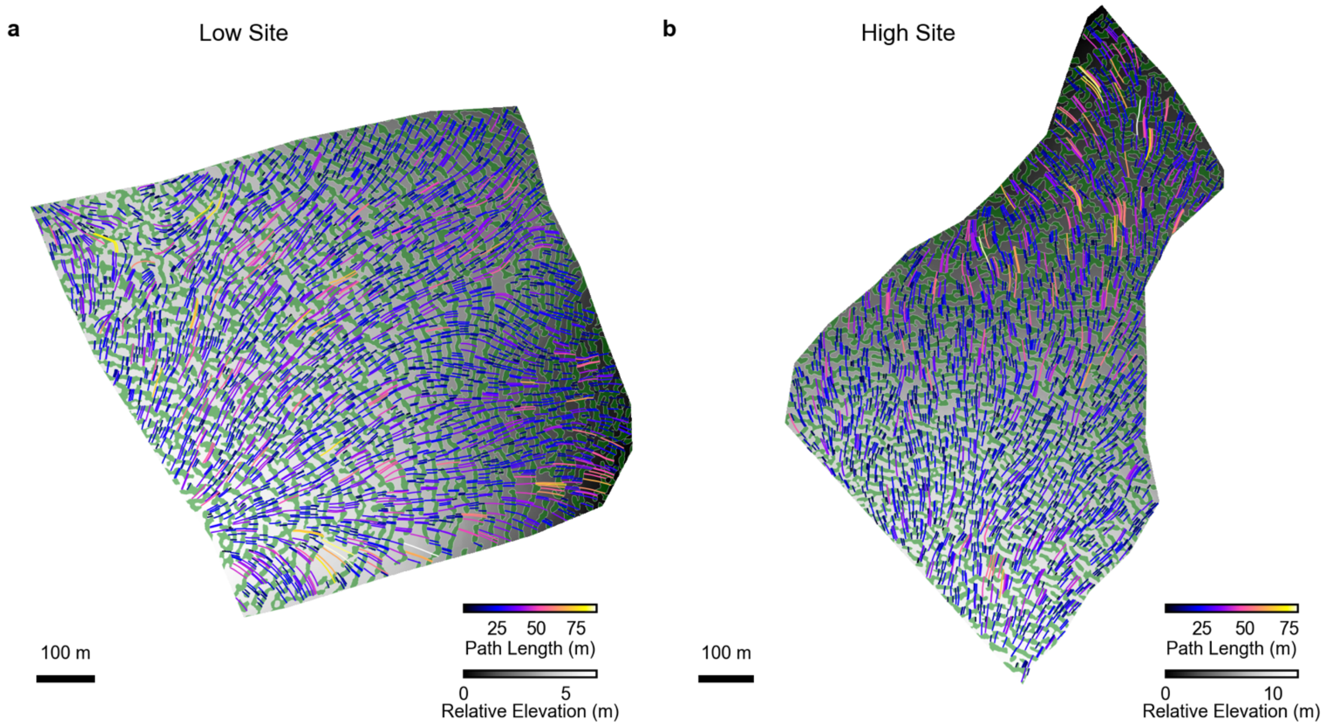

Extended Data Fig. 2: Site maps with automatically identified downslope paths. Map of the **a,** Low site and **b,** High site, showing relative elevation (grey shading) and vegetation bands (translucent green; Methods M4). Automatically defined downslope paths (only 1/20th shown for clarity; Methods M5) coloured by path length. North is orientated upwards, scale bars provided.

259

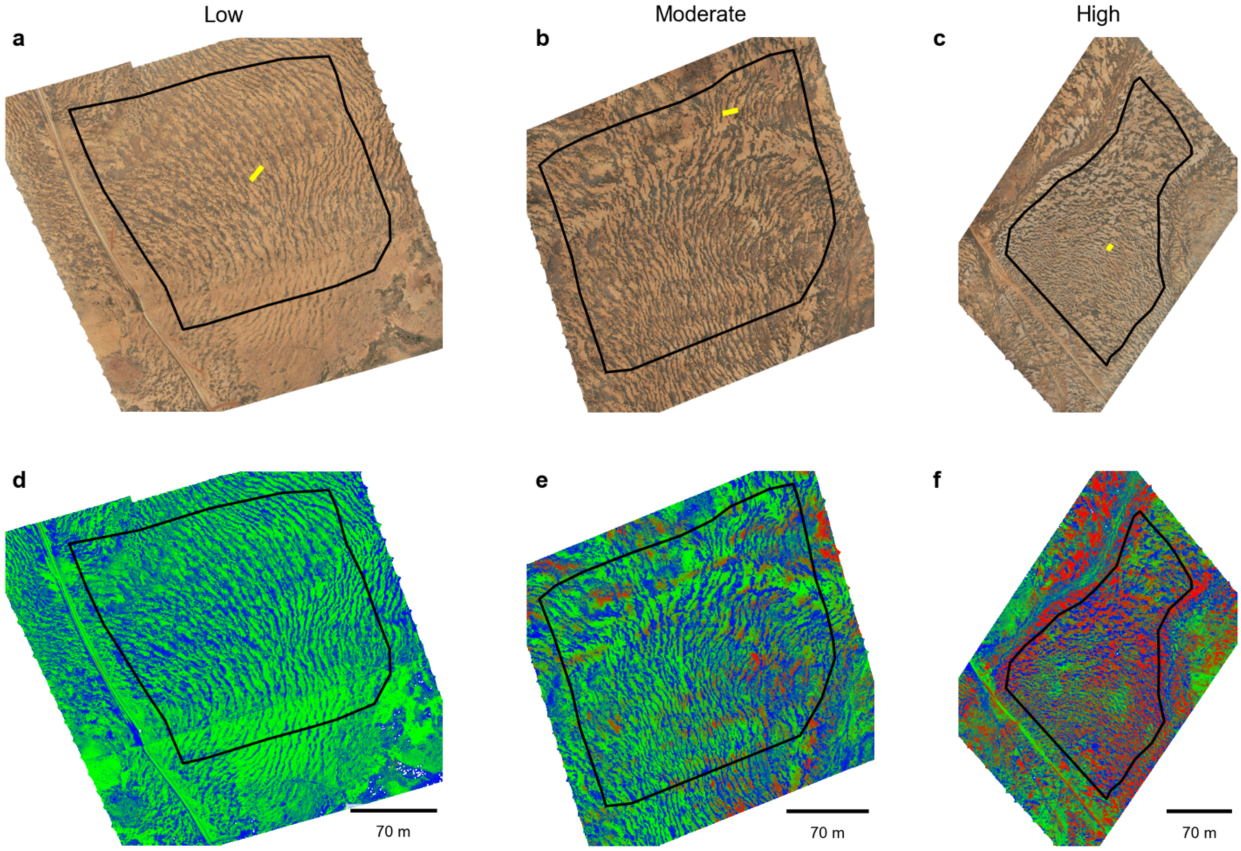

Extended Data Fig. 3: Site maps. a-c, Orthomosaic maps of each site (labelled above), gridded at 2.5-cm resolution (Methods M2). Soil sampling transects are shown (yellow line; Methods M7). **d-f,** False colour surface cover maps of each site, gridded at 5-cm resolution (Methods M3), where blue is vegetation, green is soil, and red is desert pavement. Valid survey region is shown in all panels (black outline). Scale bars provided for each site (columns).

260

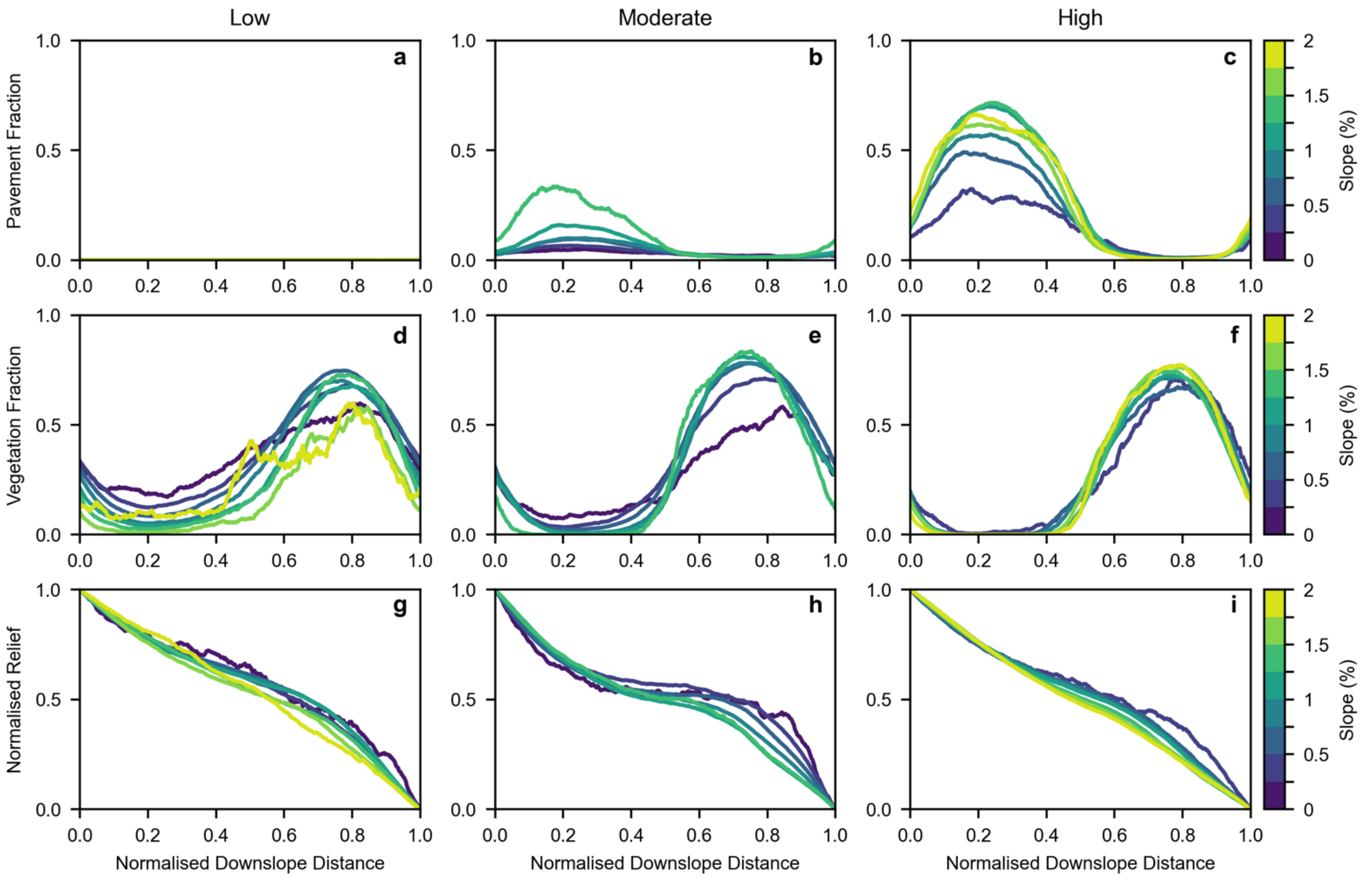

Extended Data Fig. 4: Normalised median downslope profiles. a-c, Desert pavement fraction, **d-f,** vegetation fraction, and **g-i,** normalised relief for the Low, Moderate, and High sites (columns, labelled above), binned by slope.

261

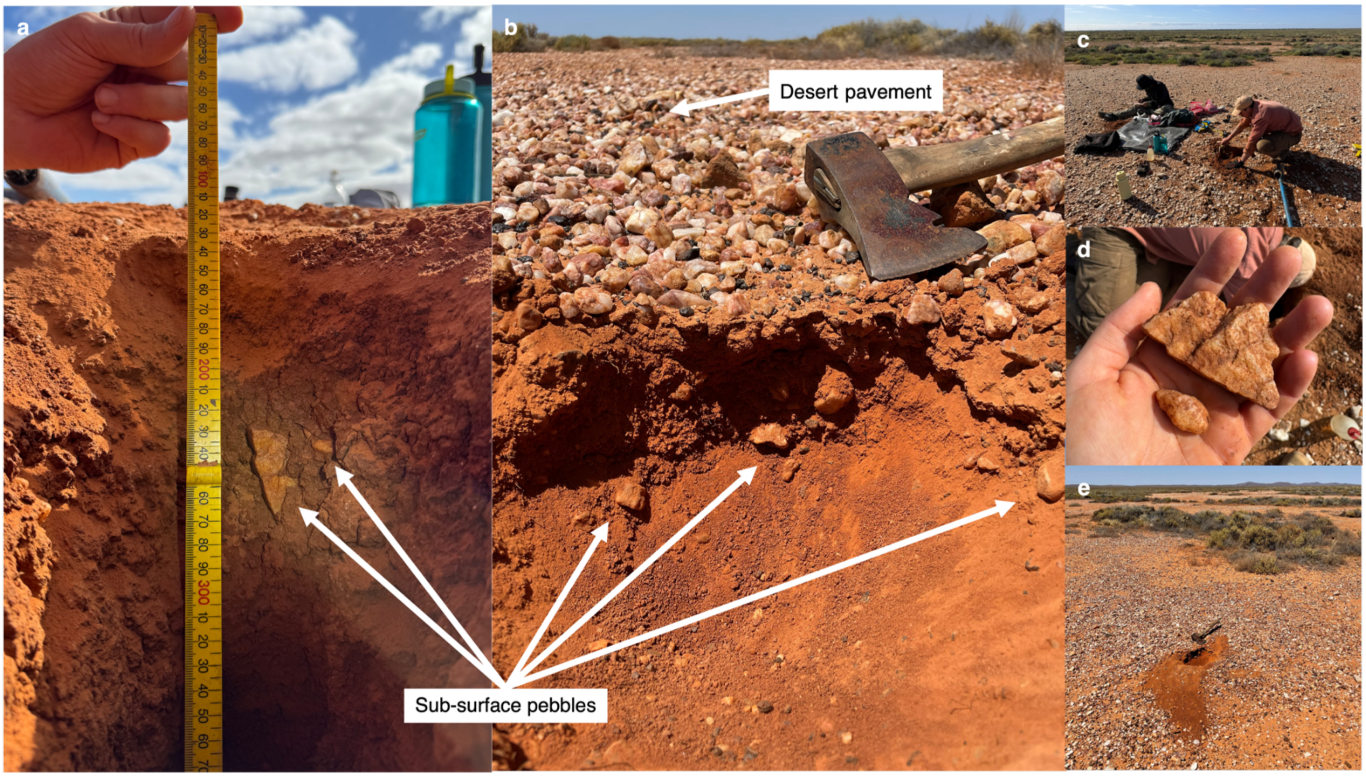

Extended Data Fig. 5: Typical sub-surface sediment profile beneath a desert pavement surface. a and b, Images of exposed sediment profiles with sub-surface pebbles labelled within the profile. A ruler is provided for scale in **a**, and a small axe (handle is ~45 cm in length) is provided in **b**. **c**, Image showing the location and size of the profile from **a**, which was dug with a hand auger. **d**, Image showing the sub-surface pebbles extracted from **a**. **e**, Image showing the location and size of the exposed profile from **b**, which was dug with a hand trowel**.** Both profiles were dug in the middle of an interband in the Moderate site.

262

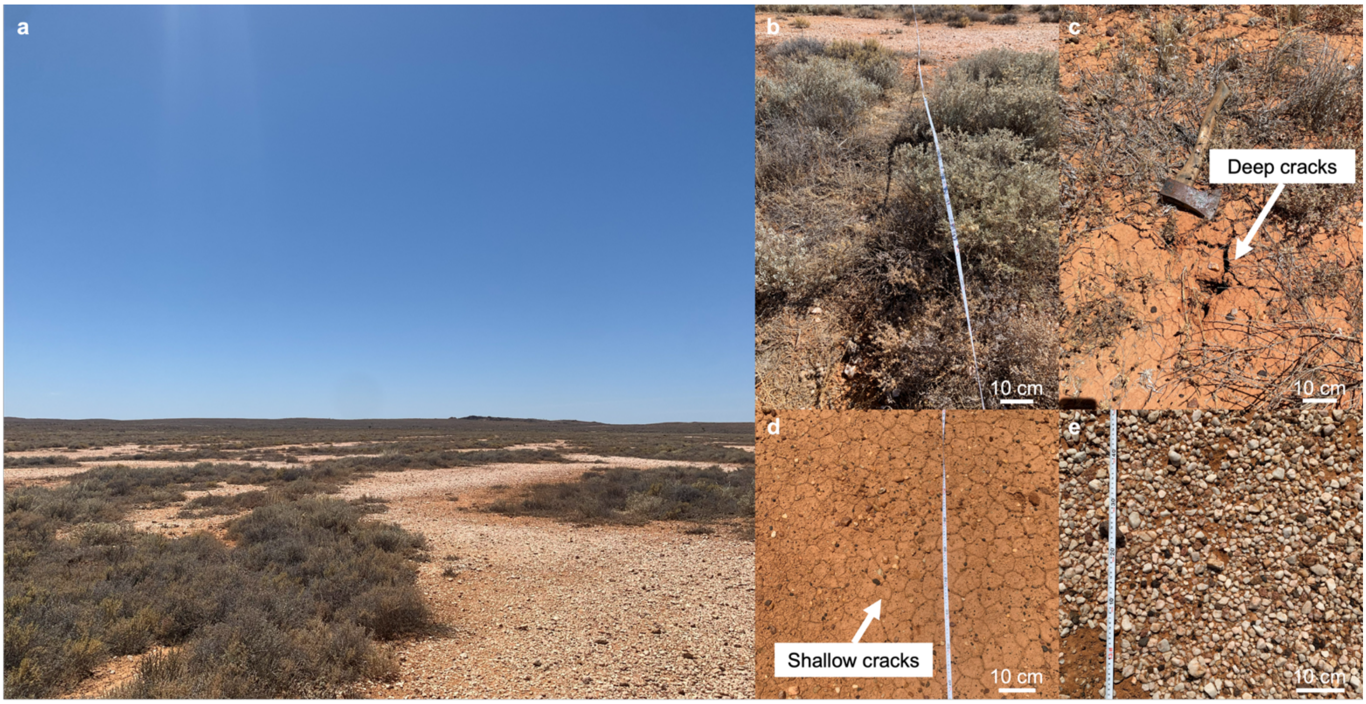

Extended Data Fig. 6: Representative band (vegetated) and interband (unvegetated) surfaces. a, Image looking along a band line (i.e., perpendicular to the slope), from the High site. **b,** Image of the typical ground cover in a vegetated band. Vegetation is predominantly *Atriplex* and *Sclerolaena* species, up to 30 cm in height. **c,** Image showing deep soil cracks visible on the surface within vegetated bands. **d,** Image of a typical surface cover in an interband where desert pavement is present. **e,** Image showing typical shallow cracks in an interband. Surficial cracking was observed in interbands where desert pavement is largely absent, and sometimes at the downslope margin of pavemented interband. Scale bars are provided in **b-e**.

263

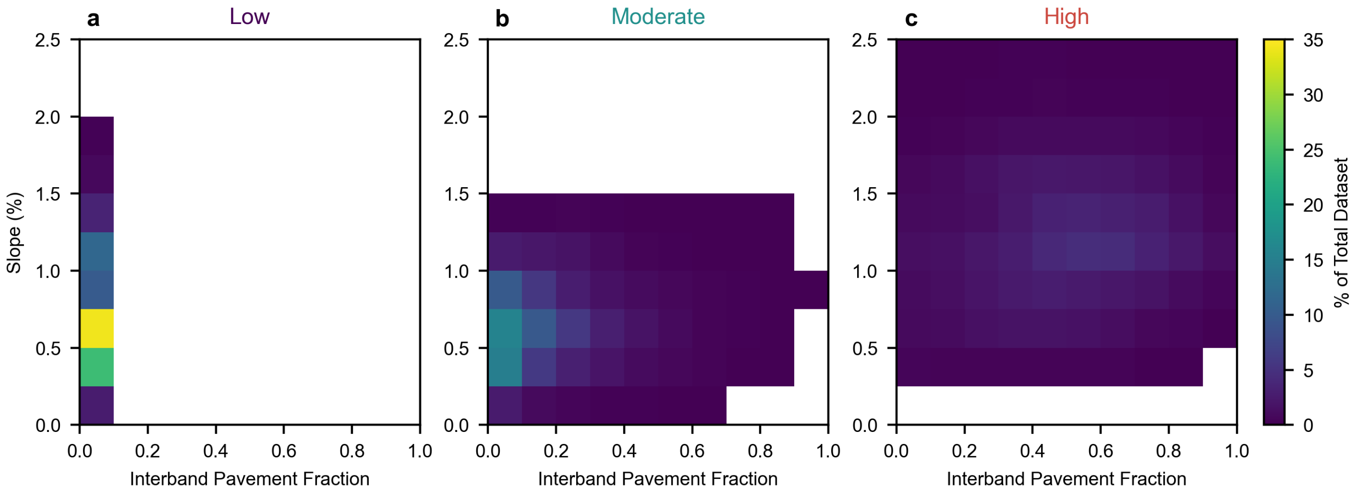

Extended Data Fig. 7: Fraction of site datasets for slope and interband pavement fraction values. Plots are coloured by the percentage of the total dataset that falls within a given slope and interband pavement fraction bin, for the **a**, Low site, **b**, Moderate site, and **c**, High site. Note that these plots show the complete dataset however in Fig. 2a-f, only bins which represent more than 0.5% of the dataset are coloured.

264

Extended Data Table 1: The fraction of downslope paths that contain less than 0.1% interband gibber fraction per site.

Site	Total Number of Paths	Paths with < 0.1% Interband Gibber Fraction	Fraction of Dataset (%)
High	57,034	3,015	5.29
Moderate	79,740	36,245	45.45
Low	67,065	58,223	86.82

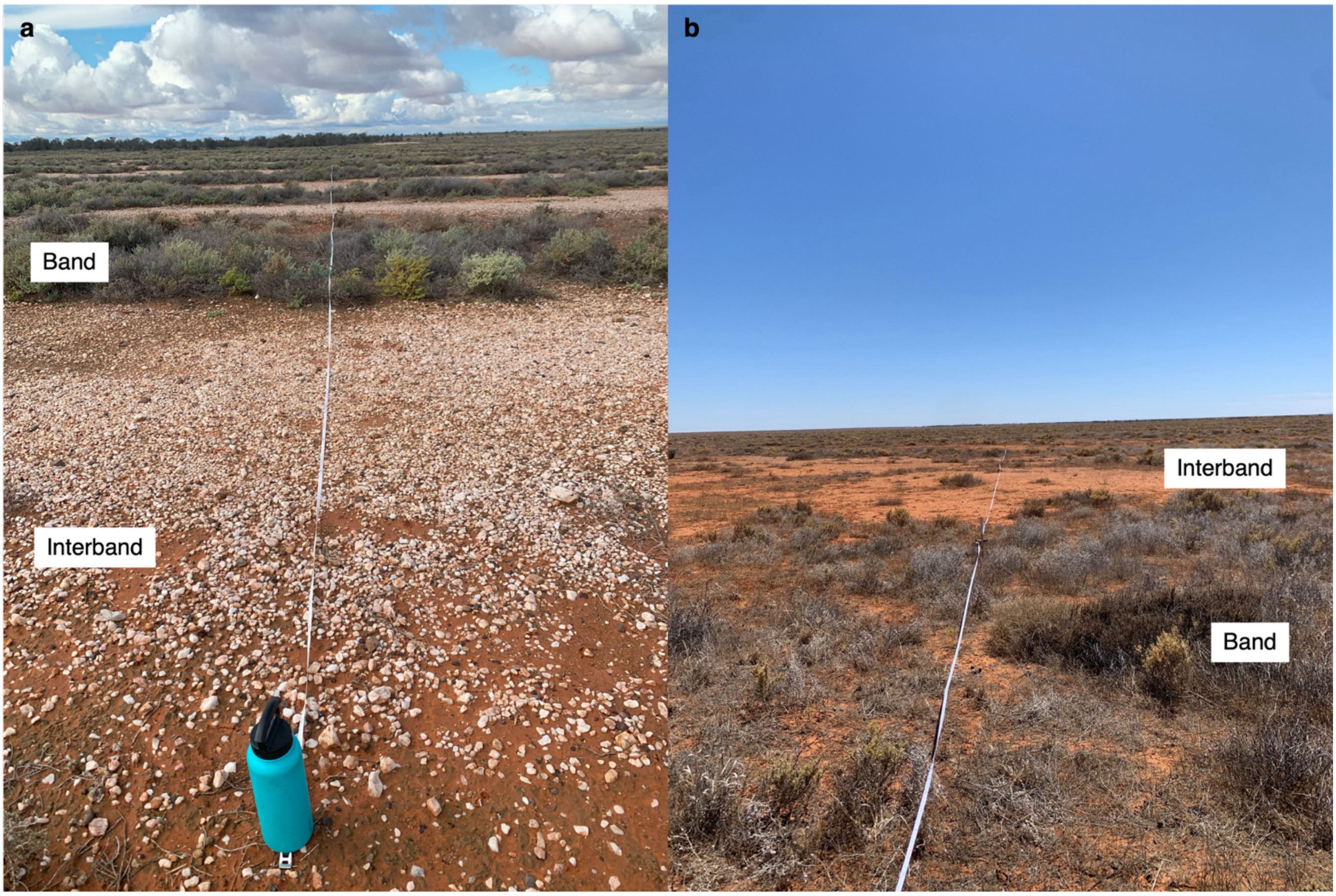

Extended Data Fig. 8: Observational evidence of desert pavement inhibiting interband vegetation growth. a, A representative interband in the High site covered with a desert pavement fraction, with no vegetation cover. **b,** A representative interband in the Low site where there is very little desert pavement, showing a relative abundance of plants. Band spacing is approximately **a,** 10 m and **b,** 30 m, respectively. Both photos are taken looking downslope.

266

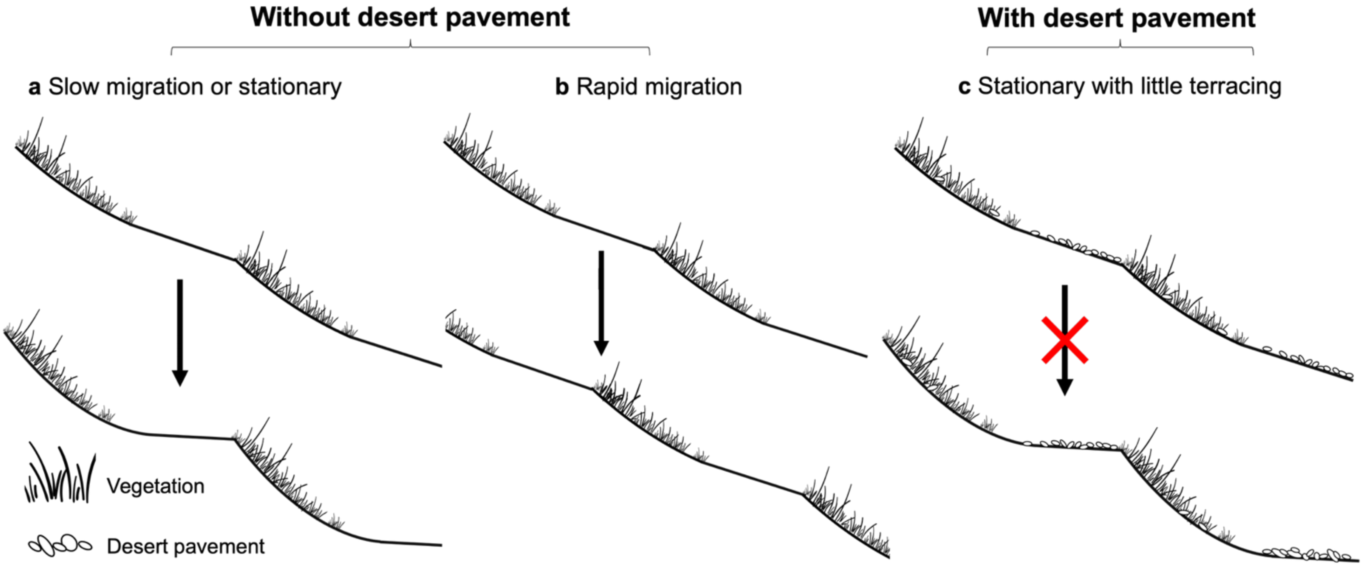

Extended Data Fig. 9: A vertically exaggerated cross-sectional schematic representation of the expected terracing development, dependent on slope, in banded vegetation sites. a, The expected development of a terracing profile in a site without desert pavement, for bands that either migrate upslope slowly relative to downslope sediment transport or remain stationary, such as in the Low site. **b,** The expected lack of terracing profile development in a site without desert pavement, for bands that migrate upslope rapidly relative to downslope sediment transport. This migration is illustrated by the offset in band and interband positions in the upslope direction as the system progresses. **c,** The expected development of a terracing profile in a site where the bands may have migrated upslope (evidence by relatively flat initial terracing profile) but are now fixed in place due to the presence of desert pavement. The absence of substantial terracing development despite this stabilisation (indicated by the red cross), as seen in the High site, suggests that desert pavement inhibits downslope sediment transport, preventing terrace development.

267